Research Article | Vol. 3, No. 8 / 15 August 2020 / OSA Continuum 2290
OSA CONTINUUM

STRATIFY: a comprehensive and versatile MATLAB code for a multilayered sphere

ILIA L. RASSKAZOV,[1,*] P. SCOTT CARNEY,[1] AND ALEXANDER MOROZ[2]

[1] The Institute of Optics, University of Rochester, Rochester, NY 14627, USA
[2] Wave-scattering.com (e-mail: wavescattering@yahoo.com)
[*] irasskaz@ur.rochester.edu

Abstract: We present a computer code for calculating near- and far-field electromagnetic properties of multilayered spheres. STRATIFY is a one-of-a-kind open-source package that allows for efficient calculation of electromagnetic near-field, energy density, total electromagnetic energy, and radiative and non-radiative decay rates of a dipole emitter located in any (non-absorbing) shell (including a host medium), and fundamental cross-sections of a multilayered sphere, all within a single program. Because of its speed and broad applicability, our package is a valuable tool for analysis of numerous light scattering problems, including but not limited to fluorescence enhancement, upconversion, downconversion, second harmonic generation, and surface enhanced Raman spectroscopy. The software is available for download from GitLab as Code 1.

1. Introduction

Multilayered spherical nanoparticles are fundamental building blocks for many vital applications in physics and chemistry: tailored scattering [1–7] and nonlinear optics [1,2,8,9], photonic crystals [10–14], sensing [15–17], photothermal cancer treatment [18–21], solar energy harvesting [22,23], photovoltaics [24], fluorescence [25–32] and upconversion [33–40] enhancement, surface-enhanced Raman scattering (SERS) [25,41,42], surface plasmon amplification by stimulated emission of radiation (spaser) [43–48], and cloaking [49–53]. To date, such matryoshkas with various combinations of dielectric and metal shells have well-established protocols for the efficient and controllable synthesis [6,54–59], greatly improved on initial synthesis attempts [3–5]. Theoretical and numerical studies in these fields are inevitable for a thoughtful design of experiment and reliable interpretation of measured data. The theory of electromagnetic light scattering from multilayered spheres has a long history since the pioneering work of Aden and Kerker for two concentric spheres [60]. An impressive number of closed-form solutions and discussions on coated [61,62] and general multilayered [63] spheres have been reported. There is a thorough understanding of scattering [64] and absorption [65] of light from multilayered spheres, including aspects for various types of illuminations [66–69], spontaneous decay rates of a dipole emitter in a presence of a multilayered sphere [26,27], electromagnetic energy [70] and near-field [71] distribution within and near the multilayered spheres, and the respective strategies for numerical implementation of the developed theories [72–75].

For a single shell, a number of features can be qualitatively understood from the quasi-static analysis [2], a full, quantitative understanding of the mechanisms underlying the applications of multilayered spheres is usually quite involved, requiring sophisticated and complex theoretical and numerical studies. The latter are often handled with commercial brute-force finite-difference time-domain (FDTD), finite-element-method (FEM) or boundary-element-method (BEM) solvers, which provide accurate results at relatively high computational price. However, spherical multilayered particles are computationally feasible *per se* due to the existence of the closed-form analytical solutions inherently convenient for computational implementation. Nonetheless, there

#399979 https://doi.org/10.1364/OSAC.399979
Journal © 2020 Received 10 Jun 2020; revised 2 Aug 2020; accepted 6 Aug 2020; published 14 Aug 2020

OSA CONTINUUM

are few *freely available*, *user-friendly* and *comprehensive* codes for light scattering from a general multilayered spheres based on these solutions [76–79]. In most of the cases, a very limited number of properties are calculated within a single freely available package. Fundamental cross-sections (i.e. scattering, absorption and extinction) and/or near fields are the usual choice implemented in freely available codes [77,80,81], and in a number of so-called "online Mie calculators" [82,83], which commonly handle only homogeneous spheres with a rare exceptions for core-shells and even more rarely for general multilayered spheres [84]. Computation of the orientation-averaged electric or magnetic field intensities (i.e. averaged over a spherical surface of a given fixed radius r), spontaneous decay rates [78] and other quantities are almost unavailable, yet generally very useful. Here we present free MATLAB code based on compact and easy-to-implement transfer-matrix formalism, which can be conveniently used to handle most of the problems of light scattering from multilayered spheres by using appropriate combinations and manipulations of transfer-matrices. The use of closed-form solutions significantly enhances the performance of the code compared with brute-force solvers without sacrificing the accuracy.

Our recursive transfer-matrix method (RTMM) has been inspired by the success of such a RTMM for *planar* stratified media developed by Abelès [85–87], summarized in Born & Wolf classical textbook [88, Sec.1.6], and can be seen as its analogue for *spherical* interfaces. From a historical perspective, the RTMM presented here had been developed as early as in 1998 and implemented in the F77 `sphere.f code` [76]. It was first applied to a number of different theoretical settings with external plane wave source [10,12,14], and successfully tested against experiment [6,13]. Later it was extended to incorporate a dipole source [26,27], energy calculations [70], and has enabled exhaustive optimization of plasmon-enhanced fluorescence [32].

The paper is organized as follows. In Sec. 2, we provide an overview of the RTMM for multilayered spheres and formulate the fundamental properties of spheres. In Sec. 3, we describe the developed code and benchmark it with robust BEM [89] implemented in freely available "MNPBEM" MATLAB package [90–93]. In Sec. 4, we discuss possible application of the code in SERS, plasmon-enhanced fluorescence, upconversion, and end with conclusive remarks and propose further developments of the package. Gaussian units are used throughout the paper.

2. Theory

2.1. Recursive transfer-matrix method

Consider a multilayered sphere with N concentric shells as shown in Fig. 1. The sphere core counts as a shell with number $n = 1$ and the host medium is the $n = N + 1$ shell. Occasionally, the host medium will be denoted as $n = h$. Each shell has the outer radius r_n and is assumed to be homogeneous and isotropic with scalar permittivity ε_n and permeability μ_n. Respective refractive indices are $\eta_n = \sqrt{\varepsilon_n \mu_n}$. We assume that the multilayered sphere is illuminated with a harmonic electromagnetic wave (either a plane wave or a dipole source) having vacuum wavelength λ. Corresponding wave vector in the n-th shell is $k_n = \eta_n \omega/c = 2\pi\eta_n/\lambda$, where c is the speed of light in vacuum, and ω is frequency. Electromagnetic fields in any shell are described by the stationary macroscopic Maxwell's equations (with time dependence $e^{-i\omega t}$ assumed and suppressed throughout the paper):

$$\mathbf{E} = \frac{ic}{\omega\varepsilon}\,(\boldsymbol{\nabla}\times\mathbf{H})\,, \qquad \mathbf{H} = -\frac{ic}{\omega\mu}\,(\boldsymbol{\nabla}\times\mathbf{E})\,. \tag{1}$$

Following the notation of [26], the basis of normalized (the normalization here refers to angular integration) *transverse* vector multipole fields $\boldsymbol{\nabla}\cdot\mathbf{F}_{pL} \equiv 0$ that satisfy the vector Helmholtz equation

$$\boldsymbol{\nabla}\times\left[\boldsymbol{\nabla}\times\mathbf{F}_{pL}(k,\mathbf{r})\right] = k^2\mathbf{F}_{pL}(k,\mathbf{r}) \tag{2}$$

OSA CONTINUUM

for n-th shell, $1 \leq n \leq N+1$, can be formed as:

$$\begin{aligned}\mathbf{F}_{ML}(k_n,\mathbf{r}) &= f_{ML}(k_n r)\mathbf{Y}_L^{(m)}(\mathbf{r})\,,\\ \mathbf{F}_{EL}(k_n,\mathbf{r}) &= \frac{1}{k_n r}\left\{\sqrt{\ell(\ell+1)}f_{EL}(k_n r)\mathbf{Y}_L^{(o)}(\mathbf{r}) + \frac{\mathrm{d}}{\mathrm{d}r}\left[r f_{EL}(k_n r)\right]\mathbf{Y}_L^{(e)}(\mathbf{r})\right\}\,,\end{aligned} \tag{3}$$

where

$$\tilde{\mathbf{F}}_{EL}(k_n,\mathbf{r}) = \frac{1}{k_n}\boldsymbol{\nabla}\times\mathbf{F}_{ML}(k_n,\mathbf{r})\,,\quad \tilde{\mathbf{F}}_{ML}(k_n,\mathbf{r}) = \frac{1}{k_n}\boldsymbol{\nabla}\times\mathbf{F}_{EL}(k_n,\mathbf{r})\,, \tag{4}$$

with $\tilde{f}_{EL} = f_{ML}$ and $\tilde{f}_{ML} = f_{EL}$. Here $L = \ell, m$ is a composite angular momentum index and f_{pL} is a suitable linear combination of spherical Bessel functions. Provided that the multipole fields in (3) represent $\mathbf{E}$, the respective subscripts $p = M$ and $p = E$ denote the *magnetic*, or *transverse electric* (TE), and *electric*, or *transverse magnetic* (TM), polarizations [94]. The so-called magnetic, $\mathbf{Y}_L^{(m)}$, longitudinal, $\mathbf{Y}_L^{(o)}$, and electric, $\mathbf{Y}_L^{(e)}$, vector spherical harmonics of degree ℓ and order m, are defined in *spherical* (φ,ϑ,r) coordinates as [80,94–96]

$$\begin{aligned}\mathbf{Y}_L^{(m)} &= i\sqrt{\frac{(\ell-m)!}{(\ell+m)!}}\sqrt{\frac{2\ell+1}{4\pi\ell(\ell+1)}}\left[\hat{\mathbf{e}}_\vartheta\frac{imP_\ell^m(\cos\vartheta)}{\sin\vartheta} - \hat{\mathbf{e}}_\varphi\frac{\mathrm{d}P_\ell^m(\cos\vartheta)}{\mathrm{d}\vartheta}\right]\exp(im\varphi)\,,\\ \mathbf{Y}_L^{(o)} &= i\sqrt{\frac{(\ell-m)!}{(\ell+m)!}}\sqrt{\frac{2\ell+1}{4\pi}}P_\ell^m(\cos\vartheta)\exp(im\varphi)\,\hat{\mathbf{e}}_r\,,\\ \mathbf{Y}_L^{(e)} &= i\sqrt{\frac{(\ell-m)!}{(\ell+m)!}}\sqrt{\frac{2\ell+1}{4\pi\ell(\ell+1)}}\left[\hat{\mathbf{e}}_\vartheta\frac{\mathrm{d}P_\ell^m(\cos\vartheta)}{\mathrm{d}\vartheta} + \hat{\mathbf{e}}_\varphi\frac{imP_\ell^m(\cos\vartheta)}{\sin\vartheta}\right]\exp(im\varphi)\,,\end{aligned} \tag{5}$$

where $\hat{\mathbf{e}}_\varphi$, $\hat{\mathbf{e}}_\vartheta$, and $\hat{\mathbf{e}}_r$ are corresponding unit vectors, and $P_\ell^m(x)$ are the associated Legendre functions of the first kind [97] of degree ℓ and order m:

$$P_\ell^m(x) = \frac{(-1)^m}{2^\ell\ell!}(1-x^2)^{m/2}\frac{\mathrm{d}^{\ell+m}}{\mathrm{d}x^{\ell+m}}(x^2-1)^\ell\,.$$

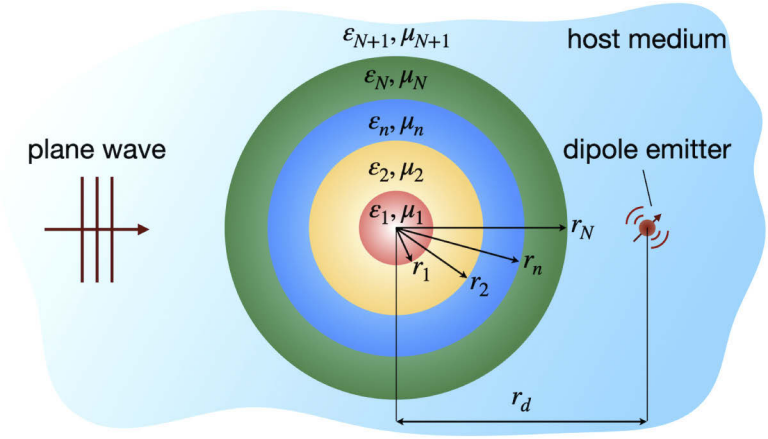

Fig. 1. A sketch of the multilayered sphere in a homogeneous isotropic host medium with permittivity $\varepsilon_h = \varepsilon_{N+1}$ and permeability $\mu_h = \mu_{N+1}$. Center of the sphere is located at the origin of the reference system.

OSA CONTINUUM

General solution for the electric field in the n-th shell, $1 \le n \le N+1$, is [26, Eq. (8)]:

$$\mathbf{E}_p(\mathbf{r}) = \sum_L \mathbf{F}_{pL}(k_n, \mathbf{r}) = \sum_L \left[A_{pL}(n)\, \mathbf{J}_{pL}(k_n, \mathbf{r}) + B_{pL}(n)\, \mathbf{H}_{pL}(k_n, \mathbf{r}) \right] . \tag{6}$$

In order to emphasize and for the sake of tracking the Bessel function dependence, the multipoles $\mathbf{F}_{pL}$ in Eq. (6) are denoted as $\mathbf{J}_{pL}$ and $\mathbf{H}_{pL}$ for the respective cases that $f_{p\ell} = j_\ell$ and $f_{p\ell} = h_\ell^{(1)}$, where j_ℓ and $h_\ell^{(1)}$ are the spherical Bessel functions of the first and third kind, correspondingly.

Given the general solution (6), the corresponding expansion of magnetic field $\mathbf{H}$ follows from that of the electric field $\mathbf{E}$ by the stationary macroscopic Maxwell's Eqs. (1) on using relations (4) [26, Eqs. (9)–(10)]:

$$\begin{aligned} \mathbf{H}_E(\mathbf{r}) &= -i\frac{\varepsilon_n}{\mu_n} \sum_L \left[A_{EL}(n)\, \mathbf{J}_{ML}(k_n, \mathbf{r}) + B_{EL}(n)\, \mathbf{H}_{ML}(k_n, \mathbf{r}) \right] , \\ \mathbf{H}_M(\mathbf{r}) &= -i\frac{\varepsilon_n}{\mu_n} \sum_L \left[A_{ML}(n)\, \mathbf{J}_{EL}(k_n, \mathbf{r}) + B_{ML}(n)\, \mathbf{H}_{EL}(k_n, \mathbf{r}) \right] . \end{aligned} \tag{7}$$

The $\mathbf{H}_{pL}$'s in Eqs. (6)–(7) with angular-momentum index L refer to a basis multipole which distinguishes them from the magnetic field $\mathbf{H}_p$.

Very much as in the case of planar stratified media [85–88], our RTMM for spherical interfaces exploits to the maximum the property that once the coefficients $A_{pL}(n+1)$ and $B_{pL}(n+1)$ on one side of a n-th shell interface are known, the coefficients $A_{pL}(n)$ and $B_{pL}(n)$ on the other side of the shell interface can be unambiguously determined, and vice versa. Schematically,

$$\begin{pmatrix} A_{pL}(n+1) \\ B_{pL}(n+1) \end{pmatrix} = T^+_{p\ell}(n) \begin{pmatrix} A_{pL}(n) \\ B_{pL}(n) \end{pmatrix} , \qquad \begin{pmatrix} A_{pL}(n) \\ B_{pL}(n) \end{pmatrix} = T^-_{p\ell}(n) \begin{pmatrix} A_{pL}(n+1) \\ B_{pL}(n+1) \end{pmatrix} , \tag{8}$$

where $T^\pm_{p\ell}(n)$ are 2×2 *transfer matrices* [26]. The matrices, which are the fundamental quantities of our approach, can be viewed as a kind of *raising* and *lowering ladder operators* of quantum mechanics. In the present case, they lower and raise the argument n of expansion coefficients $A_{pL}(n)$ and $B_{pL}(n)$. The transfer matrices are interrelated by

$$\left[T^+_{p\ell}(n) \right]^{-1} = T^-_{p\ell}(n) , \qquad \left[T^-_{p\ell}(n) \right]^{-1} = T^+_{p\ell}(n) , \tag{9}$$

and are *unambiguously* determined by matching fields across the n-th shell interface, i.e. requiring that the *tangential* components of $\mathbf{E}$ and $\mathbf{H}$ are continuous. One finds [26]:

$$T^-_{M\ell}(n) = -i \begin{pmatrix} \tilde\eta \zeta'_\ell(x)\psi_\ell(\tilde x) - \tilde\mu \zeta_\ell(x)\psi'_\ell(\tilde x) & \tilde\eta \zeta'_\ell(x)\zeta_\ell(\tilde x) - \tilde\mu \zeta_\ell(x)\zeta'_\ell(\tilde x) \\ -\tilde\eta \psi'_\ell(x)\psi_\ell(\tilde x) + \tilde\mu \psi_\ell(x)\psi'_\ell(\tilde x) & -\tilde\eta \psi'_\ell(x)\zeta_\ell(\tilde x) + \tilde\mu \psi_\ell(x)\zeta'_\ell(\tilde x) \end{pmatrix} , \tag{10}$$

$$T^-_{E\ell}(n) = -i \begin{pmatrix} \tilde\mu \zeta'_\ell(x)\psi_\ell(\tilde x) - \tilde\eta \zeta_\ell(x)\psi'_\ell(\tilde x) & \tilde\mu \zeta'_\ell(x)\zeta_\ell(\tilde x) - \tilde\eta \zeta_\ell(x)\zeta'_\ell(\tilde x) \\ -\tilde\mu \psi'_\ell(x)\psi_\ell(\tilde x) + \tilde\eta \psi_\ell(x)\psi'_\ell(\tilde x) & -\tilde\mu \psi'_\ell(x)\zeta_\ell(\tilde x) + \tilde\eta \psi_\ell(x)\zeta'_\ell(\tilde x) \end{pmatrix} , \tag{11}$$

$$T^+_{M\ell}(n) = -i \begin{pmatrix} \zeta'_\ell(\tilde x)\psi_\ell(x)/\tilde\eta - \zeta_\ell(\tilde x)\psi'_\ell(x)/\tilde\mu & \zeta'_\ell(\tilde x)\zeta_\ell(x)/\tilde\eta - \zeta_\ell(\tilde x)\zeta'_\ell(x)/\tilde\mu \\ -\psi'_\ell(\tilde x)\psi_\ell(x)/\tilde\eta + \psi_\ell(\tilde x)\psi'_\ell(x)/\tilde\mu & -\psi'_\ell(\tilde x)\zeta_\ell(x)/\tilde\eta + \psi_\ell(\tilde x)\zeta'_\ell(x)/\tilde\mu \end{pmatrix} , \tag{12}$$

$$T^+_{E\ell}(n) = -i \begin{pmatrix} \zeta'_\ell(\tilde x)\psi_\ell(x)/\tilde\mu - \zeta_\ell(\tilde x)\psi'_\ell(x)/\tilde\eta & \zeta'_\ell(\tilde x)\zeta_\ell(x)/\tilde\mu - \zeta_\ell(\tilde x)\zeta'_\ell(x)/\tilde\eta \\ -\psi'_\ell(\tilde x)\psi_\ell(x)/\tilde\mu + \psi_\ell(\tilde x)\psi'_\ell(x)/\tilde\eta & -\psi'_\ell(\tilde x)\zeta_\ell(x)/\tilde\mu + \psi_\ell(\tilde x)\zeta'_\ell(x)/\tilde\eta \end{pmatrix} , \tag{13}$$

where $\psi_\ell(x) = x j_\ell(x)$ and $\zeta_\ell(x) = x h_\ell^{(1)}(x)$ are the Riccati-Bessel functions, prime denotes the derivative with respect to the argument in parentheses, $x_n = k_n r_n$ and $\tilde x_n = x_n/\tilde\eta_n = k_{n+1} r_n$ are the

OSA CONTINUUM

internal and external dimensionless size parameters, $\tilde{\eta}_n = \eta_n/\eta_{n+1}$ and $\tilde{\mu}_n = \mu_n/\mu_{n+1}$ are relative refractive indices and permeabilities. For the sake of clarity, the n-subscript has been suppressed on the rhs of Eqs. (10)–(13). The above expressions for $T^{\pm}_{p\ell}(n)$ are general, independent on the incident field, and valid for any homogeneous and isotropic medium, including *gain* ($\Im(\varepsilon_n)<0$) or *magnetic* materials ($\mu_n \neq 1$).

The formalism becomes compact upon the use of the *composite* transfer matrices $\mathcal{T}_{p\ell}(n)$ and $\mathcal{M}_{p\ell}(n)$ defined as ordered (from the left to the right) products of the constituent *raising* and *lowering* 2×2 matrices from Eqs. (10)–(13):

$$\mathcal{T}_{p\ell}(n) = \prod_{j=n-1}^{1} T^{+}_{p\ell}(j)\,, \qquad \mathcal{M}_{p\ell}(n) = \prod_{j=n}^{N} T^{-}_{p\ell}(j)\,. \tag{14}$$

Composite matrices $\mathcal{T}_{p\ell}(n)$ and $\mathcal{M}_{p\ell}(n)$ transfer expansion coefficients to the n-th shell from the sphere core or from the surrounding medium, respectively. Note that $\mathcal{T}_{p\ell}(n)$ are defined for $2 \le n \le N+1$, while $\mathcal{M}_{p\ell}(n)$ are defined for $1 \le n \le N$. They are used in our formalism to chiefly relate the expansion coefficients in the core, or in the surrounding medium, to those in a source region. For example, for a source in the host medium $\mathcal{T}_{p\ell}(N+1)$ enables one to obviate all the intermediary shell interfaces and to relate the expansion coefficients in the core directly to those in the surrounding host medium,

$$\begin{pmatrix} A_{pL}(N+1) \\ B_{pL}(N+1) \end{pmatrix} = \mathcal{T}_{p\ell}(N+1) \begin{pmatrix} A_{pL}(1) \\ B_{pL}(1) \end{pmatrix}. \tag{15}$$

The latter formally reduces the problem of a *multilayered* sphere with a source in the host medium to that of a *homogeneous* sphere. Analogously to (9):

$$\left[\mathcal{T}_{p\ell}(N+1)\right]^{-1} = \mathcal{M}_{p\ell}(1)\,, \qquad \left[\mathcal{M}_{p\ell}(1)\right]^{-1} = \mathcal{T}_{p\ell}(N+1)\,. \tag{16}$$

The reader familiar with the RTMM for planar stratified media (e.g. multilayer coatings and interference filters) will recognize in the relations (8), (9), (14), (15), (16) familiar properties of the constituent and composite transfer matrices for planar interfaces [85–88].

In order to *unambiguously* determine the expansion coefficients $A_{pL}(n)$ and $B_{pL}(n)$ in each shell, one has to impose *two* boundary conditions, which is the subject of the following section.

2.2. Boundary conditions

The total number of different sets of expansion coefficients comprising all j's from the interval $1 \le j \le N+1$ is larger by two than the number of corresponding equations. Therefore, boundary conditions have to be imposed to unambiguously determine the expansion coefficients at any shell. They are

1. The *regularity* condition of the solution at the sphere origin, which eliminates $h^{(1)}_{\ell}(0) \to \infty$ for $f_{p\ell}$ in Eq. (3) in the core region:

$$B_{EL}(1) = B_{ML}(1) \equiv 0\,. \tag{17}$$

2. For a source located *outside* a sphere, the $A_{pL}(N+1)$ coefficients at any given frequency ω are equal to the expansion coefficients of an incident electromagnetic field in spherical coordinates.

OSA CONTINUUM

The *regularity* condition (17) alone suffices to unambiguously determine the m-independent (due to spherical symmetry of a problem) ratio [94]:

$$\mathcal{T}_{21;p\ell}(N+1)/\mathcal{T}_{11;p\ell}(N+1) = \mathbb{T}_{p\ell}, \tag{18}$$

which defines the familiar T-matrix of scattering theory, $\mathbb{T}_{p\ell}$, where i,j in $\mathcal{T}_{ij;p\ell}(n)$ label the (i,j)-th element of the 2×2 matrix $\mathcal{T}_{p\ell}(n)$. Note that $\mathbb{T}_{p\ell}$ are nothing but familiar expansion coefficients a_ℓ and b_ℓ in Bohren and Huffman's representation [80, Eqs. (4.56),(4.57)], but with the opposite sign: $\mathbb{T}_{E\ell} = -a_\ell$ and $\mathbb{T}_{M\ell} = -b_\ell$.

Corresponding closed-form analytic expressions for applying the second boundary condition are presented in (i) Refs. [70, Eq. (10)], [96] for the plane electromagnetic wave, and in (ii) Ref. [26, Eqs. (44),(50)] for the electric dipole source. In the case of an elementary dipole radiating *inside* a sphere, there is no source outside a sphere, and the second boundary condition reduces to $A_{pL}(N+1) = 0$ [26].

2.3. Far-field properties

Fundamental cross sections σ (scattering, absorption and extinction) are determined as an infinite sum over polarizations ($p = E, M$) and all partial ℓ-waves:

$$\begin{aligned}
\sigma_{\text{sca}} &= \sum_{p,\ell}\sigma_{\text{sca};p\ell} = \frac{\pi}{k_h^2}\sum_{p,\ell}(2\ell+1)\left|\mathbb{T}_{p\ell}\right|^2 ,\\
\sigma_{\text{abs}} &= \sum_{p,\ell}\sigma_{\text{abs};p\ell} = \frac{\pi}{2k_h^2}\sum_{p,\ell}(2\ell+1)\left(1-\left|1+2\mathbb{T}_{p\ell}\right|^2\right) ,\\
\sigma_{\text{ext}} &= \sum_{p,\ell}\sigma_{\text{ext};p\ell} = -\frac{2\pi}{k_h^2}\sum_{p,\ell}(2\ell+1)\,\Re\left(\mathbb{T}_{p\ell}\right) ,
\end{aligned} \tag{19}$$

where $\Re$ takes the real part, and $\mathbb{T}_{p\ell}$ is found from Eq. (18).

On using polarized scattering waves parallel and perpendicular to the scattering plane,

$$\begin{aligned}
S_{\parallel}(\vartheta) &= -\sum_{\ell}\frac{2\ell+1}{\ell(\ell+1)}\left[\mathbb{T}_{E\ell}\frac{\mathrm{d}P_\ell^1(\cos\vartheta)}{\mathrm{d}\vartheta} + \mathbb{T}_{M\ell}\frac{P_\ell^1(\cos\vartheta)}{\sin\vartheta}\right] ,\\
S_{\perp}(\vartheta) &= -\sum_{\ell}\frac{2\ell+1}{\ell(\ell+1)}\left[\mathbb{T}_{M\ell}\frac{\mathrm{d}P_\ell^1(\cos\vartheta)}{\mathrm{d}\vartheta} + \mathbb{T}_{E\ell}\frac{P_\ell^1(\cos\vartheta)}{\sin\vartheta}\right] ,
\end{aligned} \tag{20}$$

one can easily build up scattering matrix, find Stokes parameters [80, Eq. (4.77)], and obtain angle-resolved scattering pattern.

2.4. Near-field properties

For a given illumination, and, thus, known expansion coefficients $A_{pL}(n)$ and $B_{pL}(n)$, the electromagnetic field can be unambiguously defined by Eqs. (6) and (7). Below we consider more sophisticated near-field properties.

2.4.1. Electromagnetic energy

Total electromagnetic energy W stored within a multilayered sphere is a sum of energies, W_n, stored within any given n-th shell, which in turn is an integral of an electromagnetic energy

OSA CONTINUUM

density $w_n(r)$ over the n-th shell:

$$W = \sum_{n=1}^{N} W_n = \sum_{n=1}^{N} \int_{r_{n-1}}^{r_n} w_n(r) r^2 \mathrm{d}r \,, \quad w_n(r) = \frac{1}{4} \oint \left[G_e(\varepsilon_n) \left|\mathbf{E}(\mathbf{r})\right|^2 + G_m(\mu_n) \left|\mathbf{H}(\mathbf{r})\right|^2 \right] \mathrm{d}\Omega \,, \tag{21}$$

where $r_0 = 0$, i.e. the core "inner radius". Here we limit the discussion to a *plane wave* excitation. For non-dispersive (usually dielectric) shells [98], electric and magnetic coefficients in (21) are

$$G_e(\varepsilon_n) = \Re(\varepsilon_n) \,, \qquad G_m(\mu_n) = \Re(\mu_n) \,, \tag{22}$$

while for the dispersive and absorbing shells [99]:

$$G_e(\varepsilon_n, \omega) = \Re(\varepsilon_n) + \frac{2\omega}{\gamma_D} \Im(\varepsilon_n) \,, \tag{23}$$

where γ_D is the free electron damping constant in the Drude formula, and $\Im$ takes the imaginary part. In our code, we use Drude fit parameters from either Blaber et al. [100] or Ordal et al. [101].

Electric and magnetic components from Eq. (21) are nothing but the *orientation-averaged* electric and magnetic field intensities:

$$\begin{aligned} \oint |\mathbf{E}|^2 \, \mathrm{d}\Omega &= 2\pi |E_0|^2 \sum_{\ell=1}^{\infty} \left[(2\ell+1) \left|\bar{f}_{M\ell}\right|^2 + (\ell+1) \left|\bar{f}_{E,\ell-1}\right|^2 + \ell \left|\bar{f}_{E,\ell+1}\right|^2 \right] \,, \\ \oint |\mathbf{H}|^2 \, \mathrm{d}\Omega &= 2\pi |E_0|^2 \frac{|\varepsilon_n|}{|\mu_n|} \sum_{\ell=1}^{\infty} \left[(2\ell+1) \left|\bar{f}_{E\ell}\right|^2 + (\ell+1) \left|\bar{f}_{M,\ell-1}\right|^2 + \ell \left|\bar{f}_{M,\ell+1}\right|^2 \right] \,. \end{aligned} \tag{24}$$

Here $\bar{f}_{p\ell,\ell\pm1} = \bar{A}_{p\ell}(n) j_{\ell,\ell\pm1}(k_n r) + \bar{B}_{p\ell}(n) h^{(1)}_{\ell,\ell\pm1}(k_n r)$. Note that in all cases the spherical Bessel functions of either ℓ and $\ell \pm 1$ orders are multiplied by the expansions coefficients $\bar{A}_{p\ell}$ and $\bar{B}_{p\ell}$ with the index ℓ. These expansion coefficients are determined via raising $\mathcal{T}_{p\ell}(n)$ and lowering $\mathcal{M}_{p\ell}(n)$ composite transfer matrices as

$$\bar{A}_{p\ell}(n) = \begin{cases} 1/\mathcal{T}_{11;p\ell}(N+1) \,, & n = 1 \,, \\ \mathcal{M}_{11;p\ell}(n) + \mathcal{M}_{12;p\ell}(n) \dfrac{\mathcal{T}_{21;p\ell}(N+1)}{\mathcal{T}_{11;p\ell}(N+1)} \,, & 1 < n < N+1 \,, \\ 1 \,, & n = N+1 \,, \end{cases} \tag{25}$$

$$\bar{B}_{p\ell}(n) = \begin{cases} 0 \,, & n = 1 \,, \\ \mathcal{M}_{21;p\ell}(n) + \mathcal{M}_{22;p\ell}(n) \dfrac{\mathcal{T}_{21;p\ell}(N+1)}{\mathcal{T}_{11;p\ell}(N+1)} \,, & 1 < n < N+1 \,, \\ \dfrac{\mathcal{T}_{21;p\ell}(N+1)}{\mathcal{T}_{11;p\ell}(N+1)} \,, & n = N+1 \,. \end{cases} \tag{26}$$

Because the surface integrals of electric and magnetic field intensities are performed analytically [70], the calculation of average intensity costs the same computational time as determining intensity at a *single* given point.

OSA CONTINUUM

The radial integrations in (21) are performed by using Lommel's integration formulas [70]:

$$\begin{aligned}
&\int_{r_{n-1}}^{r_n} r^2 \mathrm{d}r \oint |\mathbf{E}|^2 \,\mathrm{d}\Omega = \\
&\qquad 2\pi |E_0|^2 \frac{r^3}{x^2 - x^{*2}} \sum_{\ell=1}^{\infty} \left[(2\ell+1)\bar{F}_{M\ell} + (\ell+1)\bar{F}_{E,\ell-1} + \ell \bar{F}_{E,\ell+1} \right] \Big|_{r=r_{n-1}}^{r=r_n}, \\
&\int_{r_{n-1}}^{r_n} r^2 \mathrm{d}r \oint |\mathbf{H}|^2 \,\mathrm{d}\Omega = \\
&\qquad 2\pi |E_0|^2 \frac{r^3}{x^2 - x^{*2}} \frac{|\varepsilon_n|}{|\mu_n|} \sum_{\ell=1}^{\infty} \left[(2\ell+1)\bar{F}_{E\ell} + (\ell+1)\bar{F}_{M,\ell-1} + \ell \bar{F}_{M,\ell+1} \right] \Big|_{r=r_{n-1}}^{r=r_n}.
\end{aligned} \tag{27}$$

Here $x = k_n r$, and purely *imaginary* functions $\bar{F}_{p\ell} = 2i\Im\left(x\bar{f}_{p\ell+1}(x)\bar{f}^*_{p\ell}(x)\right)$ are cancelled by purely *imaginary* $x^2 - x^{*2} = 4i\Re(x)\Im(x)$ in the denominator, which results in purely *real* integrals in (27). For a special case of *lossless* shells, the denominator $x^2 - x^{*2}$ vanishes. It can be eliminated by using l'Hôpital's rule [70] to get the following amendments in Eq. (27):

$$x^2 - x^{*2} \to 2x, \qquad \bar{F}_{p\ell} \to x\left(|\bar{f}_{p\ell}(x)|^2 + |\bar{f}_{p\ell+1}(x)|^2\right) - (2\ell+1)\Re\left(\bar{f}_{p\ell}(x)\bar{f}^*_{p\ell+1}(x)\right).$$

Substitution of (24) and (27) into (21) yields explicit expressions for the total electromagnetic energy W_n stored within each shell of the multilayered sphere and for the electromagnetic energy density $w_n(r)$. These relations are general and valid for any shell, including the $(N+1)$-th shell being a surrounding medium. For the comprehensive derivation of the equations above, we refer the Reader to the Ref. [70], which generalizes the pioneering work by Bott and Zdunkowski on homogeneous spheres [98] and subsequent follow-ups for magnetic spheres [102] and core-shells [103].

2.4.2. Spontaneous decay rates

Radiative and nonradiative decay rates (normalized with respect to $\Gamma_{\mathrm{rad};0}$, the intrinsic radiative decay rate in the absence of a multilayered sphere) for a dipole emitter located in n_d-th shell at r_d distance from a center of a sphere (see Fig. 1) are given by [26]:

$$\begin{aligned}
\frac{\Gamma^{\perp}_{\mathrm{rad}}}{\Gamma_{\mathrm{rad};0}} &= \frac{3}{2x_d^4} \mathcal{N}_{\mathrm{rad}} \sum_{\ell=1}^{\infty} \ell(\ell+1)(2\ell+1) \left|\mathcal{F}_{E\ell}(x_d)\right|^2, \\
\frac{\Gamma^{\parallel}_{\mathrm{rad}}}{\Gamma_{\mathrm{rad};0}} &= \frac{3}{4x_d^2} \mathcal{N}_{\mathrm{rad}} \sum_{\ell=1}^{\infty} (2\ell+1) \left[\left|\mathcal{F}_{M\ell}(x_d)\right|^2 + \left|\mathcal{F}'_{E\ell}(x_d)\right|^2 \right], \\
\frac{\Gamma^{\perp}_{\mathrm{nrad}}}{\Gamma_{\mathrm{rad};0}} &= \frac{3k_d^3}{2x_d^4} \mathcal{N}_{\mathrm{nrad}} \sum_{\Im(\varepsilon_a)>0} \Im(\varepsilon_a) \sum_{\ell=1}^{\infty} \ell(\ell+1)(2\ell+1) I_{E\ell;a} \left|\mathcal{D}_{E\ell;a}(x_d)\right|^2, \\
\frac{\Gamma^{\parallel}_{\mathrm{nrad}}}{\Gamma_{\mathrm{rad};0}} &= \frac{3k_d^3}{4x_d^2} \mathcal{N}_{\mathrm{nrad}} \sum_{\Im(\varepsilon_a)>0} \Im(\varepsilon_a) \sum_{\ell=1}^{\infty} (2\ell+1) \left[I_{M\ell;a} \left|\mathcal{D}_{M\ell;a}(x_d)\right|^2 + I_{E\ell;a} \left|\mathcal{D}'_{E\ell;a}(x_d)\right|^2 \right],
\end{aligned} \tag{28}$$

where $x_d = k_d r_d$ and $k_d = 2\pi\eta_d/\lambda$. Coefficients $\mathcal{N}_{\mathrm{rad}}$ and $\mathcal{N}_{\mathrm{nrad}}$ depend on whether the decay rates were normalized with respect to the radiative decay rates in infinite homogeneous medium

OSA CONTINUUM

having the refractive index of (i) the *host* or (ii) the *shell* where the dipole emitter is located:

$$\mathcal{N}_{\mathrm{rad}}^{\mathrm{host}} = \frac{\eta_d^3}{\varepsilon_d}\frac{\varepsilon_h}{\eta_h^3}\,, \quad \mathcal{N}_{\mathrm{rad}}^{\mathrm{shell}} = \left(\frac{\eta_d}{\eta_h}\right)^6\left(\frac{\varepsilon_h}{\varepsilon_d}\right)^2\,, \qquad \mathcal{N}_{\mathrm{nrad}}^{\mathrm{host}} = \frac{\eta_d^3}{\eta_h^3}\frac{\varepsilon_h}{\varepsilon_d^2}\,, \quad \mathcal{N}_{\mathrm{nrad}}^{\mathrm{shell}} = \frac{1}{\varepsilon_d}\cdot \tag{29}$$

Functions $\mathcal{F}_{p\ell}(x_d)$ and $\mathcal{D}_{p\ell;a}(x_d)$ depend on the relative position of the emitter with respect to the sphere, and to a n_a-th absorbing shell:

$$\mathcal{F}_{p\ell}(x_d) = \begin{cases} \dfrac{\psi_\ell(x_d)}{\mathcal{M}_{21;p\ell}(1)}\,, & n_d = 1\,, \\ \dfrac{\mathcal{T}_{11;p\ell}(n_d)\psi_\ell(x_d) + \mathcal{T}_{21;p\ell}(n_d)\zeta_\ell(x_d)}{\mathcal{T}_{11;p\ell}(n_d)\mathcal{M}_{22;p\ell}(n_d) - \mathcal{T}_{21;p\ell}(n_d)\mathcal{M}_{12;p\ell}(n_d)}\,, & 1{<}n_d \le N\,, \\ \psi_\ell(x_d) + \dfrac{\mathcal{T}_{21;p\ell}(N+1)}{\mathcal{T}_{11;p\ell}(N+1)}\zeta_\ell(x_d)\,, & n_d = N+1\,, \end{cases} \tag{30}$$

$$\mathcal{D}_{p\ell;a}(x_d) = \begin{cases} \dfrac{\psi_\ell(x_d)}{\mathcal{M}_{21;p\ell}(1)}\,, & n_d = 1\,, \\ \dfrac{\mathcal{T}_{11;p\ell}(n_d)\psi_\ell(x_d) + \mathcal{T}_{21;p\ell}(n_d)\zeta_\ell(x_d)}{\mathcal{T}_{11;p\ell}(n_d)\mathcal{M}_{22;p\ell}(n_d) - \mathcal{T}_{21;p\ell}(n_d)\mathcal{M}_{12;p\ell}(n_d)}\,, & 1{<}n_d{<}n_a\,, \\ \dfrac{\mathcal{M}_{22;p\ell}(n_d)\psi_\ell(x_d) + \mathcal{M}_{12;p\ell}(n_d)\zeta_\ell(x_d)}{\mathcal{T}_{11;p\ell}(n_d)\mathcal{M}_{22;p\ell}(n_d) - \mathcal{T}_{21;p\ell}(n_d)\mathcal{M}_{12;p\ell}(n_d)}\,, & n_a{<}n_d \le N\,, \\ \zeta_\ell\,(x_d)\,, & n_d = N+1\,. \end{cases} \tag{31}$$

The summation over nonradiative decay channels in Eqs. (29) includes each absorbing shell, i.e. shell with $\Im(\varepsilon_a){>}0$. Respective volume integrals $I_{E\ell;a}$ and $I_{M\ell;a}$ are

$$\begin{aligned} I_{M\ell;a} =& \frac{1}{|k_a|^2}\int_a \left|\mathcal{A}_{M\ell;a}\psi_\ell(k_a r) + \mathcal{B}_{M\ell;a}\zeta_\ell(k_a r)\right|^2 \mathrm{d}r\,, \\ I_{E\ell;a} =& \frac{\ell(\ell+1)}{|k_a|^4}\int_a \left|\mathcal{A}_{E\ell;a}\psi_\ell(k_a r) + \mathcal{B}_{E\ell;a}\zeta_\ell(k_a r)\right|^2 \frac{\mathrm{d}r}{r^2} + \\ & \frac{1}{|k_a|^2}\int_a \left|\mathcal{A}_{E\ell;a}\psi'_\ell(k_a r) + \mathcal{B}_{E\ell;a}\zeta'_\ell(k_a r)\right|^2 \mathrm{d}r\,. \end{aligned} \tag{32}$$

Here $k_a = 2\pi\eta_a/\lambda$ is the wavevector in the absorbing shell, and coefficients $\mathcal{A}_{p\ell;a}$ and $\mathcal{B}_{p\ell;a}$ are

$$\mathcal{A}_{p\ell;a} = \begin{cases} 1\,, & n_a = 1 \text{ and } n_d{<}N+1\,, \\ \mathcal{T}_{11;p\ell}(n_a)\,, & 1{<}n_a{<}n_d{<}N+1\,, \\ \mathcal{M}_{12;p\ell}(n_a)\,, & n_d{<}n_a\,, \\ \mathcal{M}_{11;p\ell}(n_a) + \mathcal{M}_{12;p\ell}(n_a)\dfrac{\mathcal{T}_{21;p\ell}(N+1)}{\mathcal{T}_{11;p\ell}(N+1)}\,, & n_d = N+1\,, \end{cases} \tag{33}$$

$$\mathcal{B}_{p\ell;a} = \begin{cases} 0\,, & n_a = 1\,, \\ \mathcal{T}_{21;p\ell}(n_a)\,, & 1{<}n_a{<}n_d{<}N+1\,, \\ \mathcal{M}_{22;p\ell}(n_a)\,, & n_d{<}n_a\,, \\ \mathcal{M}_{21;p\ell}(n_a) + \mathcal{M}_{22;p\ell}(n_a)\dfrac{\mathcal{T}_{21;p\ell}(N+1)}{\mathcal{T}_{11;p\ell}(N+1)}\,, & n_a \neq 1 \text{ and } n_d = N+1\,. \end{cases} \tag{34}$$

Note that $\mathcal{A}_{p\ell;a}$ and $\mathcal{B}_{p\ell;a}$ depend only on the *relative* position of the dipole with respect to the absorbing shell. We make use of this property to optimize calculations, namely, we get $I_{E\ell;a}$ and $I_{M\ell;a}$ once for a set of r_d, considering only the *relative* position of the dipole emitter.

For the detailed discussion of the spontaneous decay rates of a dipole emitter in a presence of a general multilayered sphere, we refer the reader to Ref. [26].

OSA CONTINUUM

2.5. Convergence criteria

Numerical implementation of equations above, which involve infinite summation over ℓ, requires truncation at some finite number $\ell_{\max}$, which, as in any Mie theory based code, determines the total number of the vector spherical wave functions involved in calculations as $2[(\ell_{\max}+1)^2-1]$. For far-field properties, Eqs. (19) and (20), the classic choice is the Wiscombe criterion [104]:

$$\ell_{\max} = \begin{cases} x_N + 4x_N^{1/3} + 1\,, & 0.02 \le x_N \le 8\,, \\ x_N + 4.05x_N^{1/3} + 2\,, & 8 < x_N\,, \end{cases} \tag{35}$$

where $x_N = k_h r_N$ is the usual size parameter. Keeping in mind plasmonics and nanophotonics applications as intended for our package, and recalling finite precision of the MATLAB, we limit the discussion for multilayered spheres with x_N<50 requiring $\ell_{\max} \lesssim 70$, which is more than sufficient.

For the near-field, Eqs. (6), (7), and for the electromagnetic energy, Eqs. (21), (24), (27), slightly larger cut-off value is recommended [105]:

$$\ell_{\max} = x_N + 11x_N^{1/3} + 1\,. \tag{36}$$

For the dipole source implied in Eq. (28), especially when considering non-radiative decay rates [26,106], the *accuracy* has to be set instead of $\ell_{\max}$, since there are no general guidelines for choosing the latter in this case.

2.6. Electron free path correction

For thin metallic shell with thickness $(r_n - r_{n-1})$ less than a free electron path, the bulk permittivity $\varepsilon_{n,\text{bulk}}$ has to be corrected to take into account electron scattering from the shell surface [107]:

$$\varepsilon_n \to \varepsilon_{n,\text{bulk}} + \frac{\omega_p^2}{\omega^2 + i\gamma_D\omega} - \frac{\omega_p^2}{\omega^2 + i\gamma\omega}\,, \quad \gamma = \gamma_D + \frac{\upsilon_F}{L_{\text{eff}}}\,, \quad L_{\text{eff}} = \frac{4}{3}\frac{r_n^3 - r_{n-1}^3}{r_n^2 + r_{n-1}^2}\,, \tag{37}$$

where υ_F is the Fermi velocity and ω_p is plasma frequency. This modification of thin metallic shells permittivity may have crucial consequences for their electromagnetic properties [20,21,108–110].

3. Computer code

3.1. Overview

Fundamental properties are calculated with the following functions:

- `t_mat.m` calculates transfer matrices with Eqs. (10)–(13) and returns their ordered products (14). Any other function which returns electromagnetic properties (decay rates, electromagnetic energy and fields, far-field properties and etc) makes use of pre-calculated ordered products of transfer matrices for a better performance;
- `decay.m` returns decay rates calculated with Eqs. (28). Decay rates are normalized (see Eqs. (29)) with respect to radiative decay rates of a dipole in a homogeneous medium (without a multilayered sphere) with the refractive index of a *shell* where the dipole is embedded, η_d, or with the refractive index of a *host*, η_h;
- `nrg_dens.m` returns normalized by the factor $\pi|E_0|^2\varepsilon_h$ [70, Sec.3E] electric and magnetic components of electromagnetic energy density, $w_n(r)$, given by Eq. (21), and orientation-averaged intensities of electric and magnetic fields given by Eq. (24);

OSA CONTINUUM

- `nrg_tot.m` returns normalized by the factor $(2/3)\pi|E_0|^2(r_n - r_{n-1}^3)\varepsilon_h$ [70, Sec.3E] electric and magnetic components of *total* electromagnetic energy W_n stored within n-th shell given by Eq. (21);
- `near_fld.m` returns electric, $\mathbf{E}(\mathbf{r}) = \mathbf{E}_E(\mathbf{r})+\mathbf{E}_M(\mathbf{r})$, and magnetic, $\mathbf{H}(\mathbf{r}) = \mathbf{H}_E(\mathbf{r})+\mathbf{H}_M(\mathbf{r})$ near-field distributions given by Eqs. (6) and (7). We take the advantage of the spherical symmetry of the problem and pre-calculate computationally expensive $\mathbf{r}$-dependent Bessel functions and $\cos\theta$-dependent associated Legendre polynomials only for *unique* values of $\mathbf{r}$ and $\cos\theta$. Usually, the amount of these *unique* $\mathbf{r}$ and $\cos\theta$ is significantly smaller than the respective *total* number of points in the rectangular mesh, which results in faster execution;
- `far_fld.m` returns polarized scattering waves from Eq. (20);
- `crs_sec.m` returns fundamental cross sections from Eq. (19);
- `el_fr_pth.m` returns corrected permittivity according to Eq. (37).

Any user-defined function or experimental data for permittivity or refractive index can be used in simulations as an input for these `.m` functions. The set of example scripts included in a package provides the respective guidelines. Suitable combinations or minor post-processing of the fundamental characteristics considered in this section may be used for almost every known application of multilayered spheres briefly discussed in Sec. 4 below.

3.2. Verification and performance

We have compared STRATIFY with freely available exact BEM-based [89] solver MNPBEM [90–93]. The latter package has been chosen for a benchmark since it is a freely available comprehensive MATLAB code capable of calculating most of the quantities considered in our code. For testing purposes, we have considered fundamental cross-sections, electric near-field distribution, and spontaneous decay rates of dipole emitter in the presence of matryoshkas composed of different combinations of Au and SiO_2 layers. It can be easily seen from Fig. 2 that our code produces for spherical particles the same results as the general-purpose BEM method, but for significantly reduced computational time. This is not surprising in view of a number of exact analytic results underlying the spherical multilayered particles which are not available for general particle shapes. Any additional layer requires generation of an extra set of Bessel functions and introduces an additional multiplication by a 2×2 matrix, which causes a linear scaling of computational time with the number of layers, N. For very large x_N an increased cut-off $\ell_{\max}$, which increases with x_N, may slow down the performance due to the necessity of calculating large sets of the Bessel functions and their derivatives.

OSA CONTINUUM

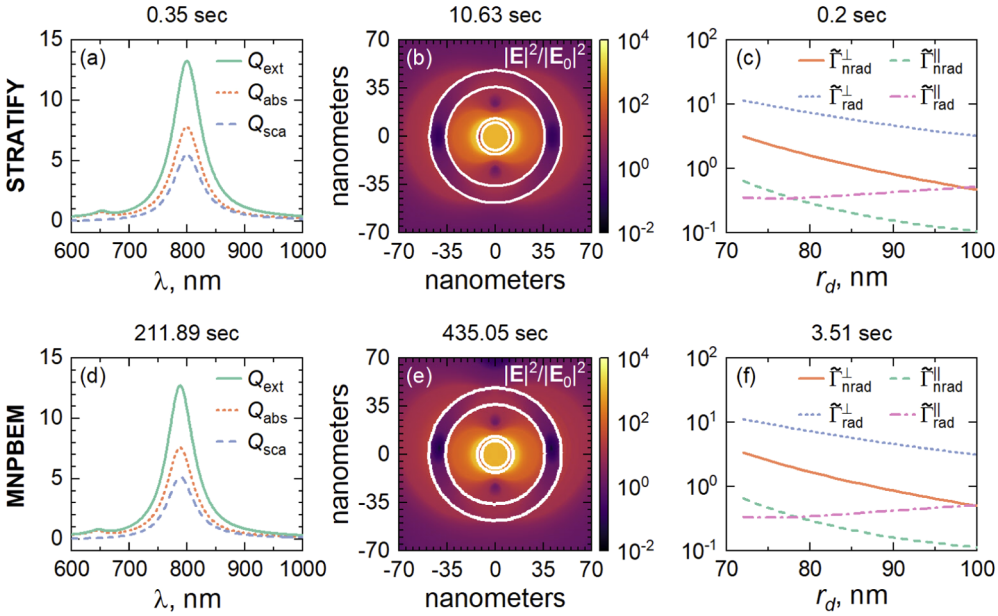

Fig. 2. Comparison between our code (top, STRATIFY) and freely available BEM-based package (bottom, MNPBEM). (a),(d) Normalized fundamental cross-section ($Q = \sigma/\pi r_2^2$) of SiO_2@Au core-shell sphere with $\{r_1, r_2\} = \{50, 55\}$ nm, in air host; (b),(e) intensity of the electric field for SiO_2@Au@SiO_2@Au matryoshka with $\{r_1, r_2, r_3, r_4\} = \{10, 13, 36, 48\}$ nm, in water host, at $\lambda = 690$ nm [111, cf. Fig. 3(b)]; (c),(f) normalized spontaneous decay rates ($\tilde{\Gamma} = \Gamma/\Gamma_{rad;0}$) for the dipole emitter located at r_d distance from the center of Au@SiO_2 core-shell sphere with $\{r_1, r_2\} = \{50, 70\}$ nm, in water host, at $\lambda = 614$ nm. Run times of codes on a laptop with 2.6 GHz 6-Core Intel Core i7 processor are shown on top of each plot. For a fair comparison, the same number of points for λ (801) in (a),(c), same 700×700 mesh in (b),(e), and same number of points for r_d (29) in (c),(f) are used. Cut-offs $\ell_{max} = 4$ and $\ell_{max} = 10$ are used in (a) and (b), according to Eq. (35) and Eq. (36), respectively, while decay rates in (c) are calculated with 0.01 accuracy. Note typically more than 50 times faster speed of our package compared to the freely available BEM-based package.

OSA CONTINUUM

4. Discussion and conclusions

The developed package is ready to be applied in a number of well-established applications of multilayered spheres in optics and photonics. Below we discuss the most common examples. Due to enormous electric field enhancement in multilayered metal-dielectric nanospheres, they are considered as good candidates for a number of applications. Squared electric field intensities from Eq. (24) or Eq. (27) are measure for performance of nanostructures in SERS [25,41,42,112–114] and second harmonic generation [8,9]. For fluorescence or upconversion enhancement, where the spontaneous decay rates of the dipole emitters are modified, the generic enhancement factor is nothing but a product of excitation rate enhancement (at excitation wavelength, λ_{exc}) and quantum yield (at emission wavelength, λ_{ems}):

$$F = \frac{\gamma_{\text{exc}}}{\gamma_{\text{exc;0}}}\frac{q_{\text{ems}}}{q_{\text{ems;0}}}, \qquad q_{\text{ems}} = \frac{\Gamma_{\text{rad}}/\Gamma_{\text{rad;0}}}{\Gamma_{\text{rad}}/\Gamma_{\text{rad;0}} + \Gamma_{\text{nrad}}/\Gamma_{\text{rad;0}} + (1-q_{\text{ems;0}})/q_{\text{ems;0}}}. \tag{38}$$

Here $\gamma_{\text{exc}}/\gamma_{\text{exc;0}} \propto |\mathbf{E}|^{2\mathcal{P}}/|\mathbf{E}_0|^{2\mathcal{P}}$, $\mathcal{P}$ is the number of photons involved in the excitation process ($\mathcal{P} = 1$ for fluorescence enhancement, $\mathcal{P} = 2$ for the upconversion), $q_{\text{ems;0}}$ is the intrinsic quantum yield of the emitter, and $\Gamma_{\text{rad, nrad}} = (2\Gamma^{\parallel}_{\text{rad, nrad}} + \Gamma^{\perp}_{\text{rad, nrad}})/3$ is an orientationally averaged decay rate determined at a fixed dipole radial position by averaging over all possible orientations of a dipole emitter. Orientationally averaged fields in γ_{exc}, and orientationally averaged decay rates, $\Gamma_{\text{rad, nrad}}$, are reasonable choice for reliable estimates, unless, of course, the emitter is positioned with a controllable orientation of its electric dipole moment at a particular (e.g. a hot spot) location.

Cloaking, Kerker effect [115], super- or optimally tuned scattering [52,116–118] and absorption [20,52,118,119], embedded photonic eigenvalues [120], spasing [44,47,121] and other intriguing phenomena [122] are easily understood from fundamental cross sections (19) and scattering patterns (20).

We have summarized a self-consistent and comprehensive RTMM theory reported earlier in our [26,70] for electromagnetic light scattering from general multilayered spheres composed of isotropic shells. Within the framework of RTMM, we have developed an efficient multi-purpose MATLAB package for calculating fundamental properties of multilayered spheres. Our package is one-of-a-kind freely available software which allows for a simultaneous calculation of a wide range of electromagnetic properties and is ready to be used for a broad number of applications in chemistry, optics and photonics, including optimization problems and machine-learning studies. We hope that the generalization presented here and corresponding MATLAB code will serve as a useful tool for photonics, physics, chemistry and other scientific communities and will boost the researches involving various kinds of multilayered spheres.

Extensions of our code for ultra-thin metallic shell characterized by nonlocal dielectric functions [123–127], an optically active shells [128–130], or including perfectly conducting boundary conditions at the sphere core are, following the theory developed in Ref. [26], rather straightforward. Further generalization of the package may include illumination with focused, Gaussian, or other beams [66–69]. An incorporation of *magnetic* dipole emitters [131–133] or modeling the effect of a multilayered sphere on the far-field radiation directivity of a dipole antenna should follow soon.

Disclosures

The authors declare no conflicts of interest.

The data for this work is available as Code 1 [134].

References

1. A. E. Neeves and M. H. Birnboim, "Composite structures for the enhancement of nonlinear optical materials," Opt. Lett. **13**(12), 1087–1089 (1988).

OSA CONTINUUM

2. A. E. Neeves and M. H. Birnboim, "Composite structures for the enhancement of nonlinear-optical susceptibility," J. Opt. Soc. Am. B **6**(4), 787–796 (1989).
3. H. S. Zhou, I. Honma, H. Komiyama, and J. W. Haus, "Controlled synthesis and quantum-size effect in gold-coated nanoparticles," Phys. Rev. B **50**(16), 12052–12056 (1994).
4. R. D. Averitt, D. Sarkar, and N. J. Halas, "Plasmon resonance shifts of Au-coated Au2S nanoshells: Insight into multicomponent nanoparticle growth," Phys. Rev. Lett. **78**(22), 4217–4220 (1997).
5. S. Oldenburg, R. Averitt, S. Westcott, and N. Halas, "Nanoengineering of optical resonances," Chem. Phys. Lett. **288**(2-4), 243–247 (1998).
6. C. Graf and A. van Blaaderen, "Metallodielectric colloidal core-shell particles for photonic applications," Langmuir **18**(2), 524–534 (2002).
7. K. Hasegawa, C. Rohde, and M. Deutsch, "Enhanced surface-plasmon resonance absorption in metal-dielectric-metal layered microspheres," Opt. Lett. **31**(8), 1136–1138 (2006).
8. Y. Pu, R. Grange, C.-L. Hsieh, and D. Psaltis, "Nonlinear optical properties of core-shell nanocavities for enhanced second-harmonic generation," Phys. Rev. Lett. **104**(20), 207402 (2010).
9. S. A. Scherbak and A. A. Lipovskii, "Understanding the second-harmonic generation enhancement and behavior in metal core-dielectric shell nanoparticles," J. Phys. Chem. C **122**(27), 15635–15645 (2018).
10. A. Moroz and C. Sommers, "Photonic band gaps of three-dimensional face-centred cubic lattices," J. Phys.: Condens. Matter **11**(4), 997–1008 (1999).
11. W. Y. Zhang, X. Y. Lei, Z. L. Wang, D. G. Zheng, W. Y. Tam, C. T. Chan, and P. Sheng, "Robust photonic band gap from tunable scatterers," Phys. Rev. Lett. **84**(13), 2853–2856 (2000).
12. A. Moroz, "Photonic crystals of coated metallic spheres," Europhys. Lett. **50**(4), 466–472 (2000).
13. K. P. Velikov, A. Moroz, and A. Van Blaaderen, "Photonic crystals of core-shell colloidal particles," Appl. Phys. Lett. **80**(1), 49–51 (2002).
14. A. Moroz, "Metallo-dielectric diamond and zinc-blende photonic crystals," Phys. Rev. B **66**(11), 115109 (2002).
15. G. Raschke, S. Brogl, A. S. Susha, A. L. Rogach, T. A. Klar, J. Feldmann, B. Fieres, N. Petkov, T. Bein, A. Nichtl, and K. Kürzinger, "Gold nanoshells improve single nanoparticle molecular sensors," Nano Lett. **4**(10), 1853–1857 (2004).
16. P. K. Jain and M. A. El-Sayed, "Surface plasmon resonance sensitivity of metal nanostructures: Physical basis and universal scaling in metal nanoshells," J. Phys. Chem. C **111**(47), 17451–17454 (2007).
17. M. A. Ochsenkühn, P. R. T. Jess, H. Stoquert, K. Dholakia, and C. J. Campbell, "Nanoshells for surface-enhanced Raman spectroscopy in Eukaryotic cells: Cellular response and sensor development," ACS Nano **3**(11), 3613–3621 (2009).
18. L. R. Hirsch, R. J. Stafford, J. A. Bankson, S. R. Sershen, B. Rivera, R. E. Price, J. D. Hazle, N. J. Halas, and J. L. West, "Nanoshell-mediated near-infrared thermal therapy of tumors under magnetic resonance guidance," Proc. Natl. Acad. Sci. **100**(23), 13549–13554 (2003).
19. C. Ayala-Orozco, C. Urban, M. W. Knight, A. S. Urban, O. Neumann, S. W. Bishnoi, S. Mukherjee, A. M. Goodman, H. Charron, T. Mitchell, M. Shea, R. Roy, S. Nanda, R. Schiff, N. J. Halas, and A. Joshi, "Au nanomatryoshkas as efficient near-infrared photothermal transducers for cancer treatment: benchmarking against nanoshells," ACS Nano **8**(6), 6372–6381 (2014).
20. V. I. Zakomirnyi, I. L. Rasskazov, S. V. Karpov, and S. P. Polyutov, "New ideally absorbing Au plasmonic nanostructures for biomedical applications," J. Quant. Spectrosc. Radiat. Transfer **187**, 54–61 (2017).
21. A. S. Kostyukov, A. E. Ershov, V. S. Gerasimov, S. A. Filimonov, I. L. Rasskazov, and S. V. Karpov, "Super-efficient laser hyperthermia of malignant cells with core-shell nanoparticles based on alternative plasmonic materials," J. Quant. Spectrosc. Radiat. Transfer **236**, 106599 (2019).
22. A. D. Phan, N. B. Le, N. T. H. Lien, and K. Wakabayashi, "Multilayered plasmonic nanostructures for solar energy harvesting," J. Phys. Chem. C **122**(34), 19801–19806 (2018).
23. Z. Wang, X. Quan, Z. Zhang, and P. Cheng, "Optical absorption of carbon-gold core-shell nanoparticles," J. Quant. Spectrosc. Radiat. Transfer **205**, 291–298 (2018).
24. X. Xu, A. Dutta, J. Khurgin, A. Wei, V. M. Shalaev, and A. Boltasseva, "TiN@TiO2 core-shell nanoparticles as plasmon-enhanced photosensitizers: The role of hot electron injection," Laser Photonics Rev. **14**(5), 1900376 (2020).
25. H. Chew, P. J. McNulty, and M. Kerker, "Model for Raman and fluorescent scattering by molecules embedded in small particles," Phys. Rev. A **13**(1), 396–404 (1976).
26. A. Moroz, "A recursive transfer-matrix solution for a dipole radiating inside and outside a stratified sphere," Ann. Phys. **315**(2), 352–418 (2005).
27. A. Moroz, "Spectroscopic properties of a two-level atom interacting with a complex spherical nanoshell," Chem. Phys. **317**(1), 1–15 (2005).
28. O. G. Tovmachenko, C. Graf, D. J. van den Heuvel, A. van Blaaderen, and H. C. Gerritsen, "Fluorescence enhancement by metal-core/silica-shell nanoparticles," Adv. Mater. **18**(1), 91–95 (2006).
29. J. Zhang, I. Gryczynski, Z. Gryczynski, and J. R. Lakowicz, "Dye-labeled silver nanoshell-bright particle," J. Phys. Chem. B **110**(18), 8986–8991 (2006).
30. C. Ayala-Orozco, J. G. Liu, M. W. Knight, Y. Wang, J. K. Day, P. Nordlander, and N. J. Halas, "Fluorescence enhancement of molecules inside a gold nanomatryoshka," Nano Lett. **14**(5), 2926–2933 (2014).

OSA CONTINUUM

31. N. Sakamoto, T. Onodera, T. Dezawa, Y. Shibata, and H. Oikawa, "Highly enhanced emission of visible light from core-dual-shell-type hybridized nanoparticles," Part. Part. Syst. Charact. **34**(12), 1700258 (2017).
32. S. Sun, I. L. Rasskazov, P. S. Carney, T. Zhang, and A. Moroz, "Critical role of shell in enhanced fluorescence of metal-dielectric core-shell nanoparticles," J. Phys. Chem. C **124**(24), 13365–13373 (2020).
33. F. Zhang, G. B. Braun, Y. Shi, Y. Zhang, X. Sun, N. O. Reich, D. Zhao, and G. Stucky, "Fabrication of Ag@SiO2@Y2O3:Er nanostructures for bioimaging: Tuning of the upconversion fluorescence with silver nanoparticles," J. Am. Chem. Soc. **132**(9), 2850–2851 (2010).
34. A. Priyam, N. M. Idris, and Y. Zhang, "Gold nanoshell coated NaYF4 nanoparticles for simultaneously enhanced upconversion fluorescence and darkfield imaging," J. Mater. Chem. **22**(3), 960–965 (2012).
35. P. Yuan, Y. H. Lee, M. K. Gnanasammandhan, Z. Guan, Y. Zhang, and Q.-H. Xu, "Plasmon enhanced upconversion luminescence of NaYF4:Yb,Er@SiO2@Ag core-shell nanocomposites for cell imaging," Nanoscale **4**(16), 5132–5137 (2012).
36. P. Kannan, F. A. Rahim, X. Teng, R. Chen, H. Sun, L. Huang, and D.-H. Kim, "Enhanced emission of NaYF4:Yb,Er/Tm nanoparticles by selective growth of Au and Ag nanoshells," RSC Adv. **3**(21), 7718 (2013).
37. Y. Ding, X. Zhang, H. Gao, S. Xu, C. Wei, and Y. Zhao, "Plasmonic enhanced upconversion luminescence of β-NaYF4:Yb3+/Er3+ with Ag@SiO2 core-shell nanoparticles," J. Lumin. **147**, 72–76 (2014).
38. W. Xu, X. Min, X. Chen, Y. Zhu, P. Zhou, S. Cui, S. Xu, L. Tao, and H. Song, "Ag-SiO2-Er2O3 nanocomposites: Highly effective upconversion luminescence at high power excitation and high temperature," Sci. Rep. **4**(1), 5087 (2015).
39. Z. Wang, W. Gao, R. Wang, J. Shao, Q. Han, C. Wang, J. Zhang, T. Zhang, J. Dong, and H. Zheng, "Influence of SiO2 layer on the plasmon quenched upconversion luminescence emission of core-shell NaYF4:Yb,Er@SiO2@Ag nanocomposites," Mater. Res. Bull. **83**, 515–521 (2016).
40. I. L. Rasskazov, L. Wang, C. J. Murphy, R. Bhargava, and P. S. Carney, "Plasmon-enhanced upconversion: engineering enhancement and quenching at nano and macro scales," Opt. Mater. Express **8**(12), 3787–3804 (2018).
41. D.-K. Lim, K.-S. Jeon, J.-H. Hwang, H. Kim, S. Kwon, Y. D. Suh, and J.-M. Nam, "Highly uniform and reproducible surface-enhanced Raman scattering from DNA-tailorable nanoparticles with 1-nm interior gap," Nat. Nanotechnol. **6**(7), 452–460 (2011).
42. J.-F. Li, Y.-J. Zhang, S.-Y. Ding, R. Panneerselvam, and Z.-Q. Tian, "Core-shell nanoparticle-enhanced Raman spectroscopy," Chem. Rev. **117**(7), 5002–5069 (2017).
43. M. A. Noginov, G. Zhu, A. M. Belgrave, R. Bakker, V. M. Shalaev, E. E. Narimanov, S. Stout, E. Herz, T. Suteewong, and U. Wiesner, "Demonstration of a spaser-based nanolaser," Nature **460**(7259), 1110–1112 (2009).
44. N. Calander, D. Jin, and E. M. Goldys, "Taking plasmonic core-shell nanoparticles toward laser threshold," J. Phys. Chem. C **116**(13), 7546–7551 (2012).
45. D. G. Baranov, E. Andrianov, A. P. Vinogradov, and A. A. Lisyansky, "Exactly solvable toy model for surface plasmon amplification by stimulated emission of radiation," Opt. Express **21**(9), 10779–10791 (2013).
46. N. Arnold, C. Hrelescu, and T. A. Klar, "Minimal spaser threshold within electrodynamic framework: Shape, size and modes," Ann. Phys. **528**(3-4), 295–306 (2016).
47. N. Passarelli, R. A. Bustos-Marún, and E. A. Coronado, "Spaser and optical amplification conditions in gold-coated active nanoparticles," J. Phys. Chem. C **120**(43), 24941–24949 (2016).
48. E. I. Galanzha, R. Weingold, D. A. Nedosekin, M. Sarimollaoglu, J. Nolan, W. Harrington, A. S. Kuchyanov, R. G. Parkhomenko, F. Watanabe, Z. Nima, A. S. Biris, A. I. Plekhanov, M. I. Stockman, and V. P. Zharov, "Spaser as a biological probe," Nat. Commun. **8**(1), 15528 (2017).
49. A. Alù and N. Engheta, "Multifrequency optical invisibility cloak with layered plasmonic shells," Phys. Rev. Lett. **100**(11), 113901 (2008).
50. F. Monticone, C. Argyropoulos, and A. Alù, "Multilayered plasmonic covers for comblike scattering response and optical tagging," Phys. Rev. Lett. **110**(11), 113901 (2013).
51. K. Ladutenko, O. Peña-Rodríguez, I. Melchakova, I. Yagupov, and P. Belov, "Reduction of scattering using thin all-dielectric shells designed by stochastic optimizer," J. Appl. Phys. **116**(18), 184508 (2014).
52. A. Sheverdin and C. Valagiannopoulos, "Core-shell nanospheres under visible light: Optimal absorption, scattering, and cloaking," Phys. Rev. B **99**(7), 075305 (2019).
53. K. L. Tsakmakidis, O. Reshef, E. Almpanis, G. P. Zouros, E. Mohammadi, D. Saadat, F. Sohrabi, N. Fahimi-Kashani, D. Etezadi, R. W. Boyd, and H. Altug, "Ultrabroadband 3D invisibility with fast-light cloaks," Nat. Commun. **10**(1), 4859 (2019).
54. L. R. Hirsch, A. M. Gobin, A. R. Lowery, F. Tam, R. A. Drezek, N. J. Halas, and J. L. West, "Metal nanoshells," Ann. Biomed. Eng. **34**(1), 15–22 (2006).
55. B. Jankiewicz, D. Jamiola, J. Choma, and M. Jaroniec, "Silica-metal core-shell nanostructures," Adv. Colloid Interface Sci. **170**(1-2), 28–47 (2012).
56. J. L. Montaño-Priede, O. Peña-Rodríguez, and U. Pal, "Near-electric-field tuned plasmonic Au@SiO2 and Ag@SiO2 nanoparticles for efficient utilization in luminescence enhancement and surface-enhanced spectroscopy," J. Phys. Chem. C **121**(41), 23062–23071 (2017).
57. J. L. Montaño-Priede, J. P. Coelho, A. Guerrero-Martínez, O. Peña-Rodríguez, and U. Pal, "Fabrication of monodispersed Au@SiO2 nanoparticles with highly stable silica layers by ultrasound-assisted Stöber method," J. Phys. Chem. C **121**(17), 9543–9551 (2017).

OSA CONTINUUM

58. P. Wang, A. V. Krasavin, F. N. Viscomi, A. M. Adawi, J.-S. G. Bouillard, L. Zhang, D. J. Roth, L. Tong, and A. V. Zayats, "Metaparticles: dressing nano-objects with a hyperbolic coating," Laser Photonics Rev. **12**(11), 1800179 (2018).
59. J. C. Castro-Palacio, K. Ladutenko, A. Prada, G. González-Rubio, P. Díaz-Núñez, A. Guerrero-Martínez, P. Fernández de Córdoba, J. Kohanoff, J. M. Perlado, O. Peña-Rodríguez, and A. Rivera, "Hollow Gold Nanoparticles Produced by Femtosecond Laser Irradiation," J. Phys. Chem. Lett. **11**(13), 5108–5114 (2020).
60. A. L. Aden and M. Kerker, "Scattering of electromagnetic waves from two concentric spheres," J. Appl. Phys. **22**(10), 1242–1246 (1951).
61. T. Kaiser, S. Lange, and G. Schweiger, "Structural resonances in a coated sphere: investigation of the volume-averaged source function and resonance positions," Appl. Opt. **33**(33), 7789 (1994).
62. J. A. Lock, J. M. Jamison, and C.-Y. Lin, "Rainbow scattering by a coated sphere," Appl. Opt. **33**(21), 4677 (1994).
63. J. Sinzig and M. Quinten, "Scattering and absorption by spherical multilayer particles," Appl. Phys. A: Solids Surf. **58**(2), 157–162 (1994).
64. R. Bhandari, "Scattering coefficients for a multilayered sphere: analytic expressions and algorithms," Appl. Opt. **24**(13), 1960–1967 (1985).
65. D. W. Mackowski, R. A. Altenkirch, and M. P. Menguc, "Internal absorption cross sections in a stratified sphere," Appl. Opt. **29**(10), 1551–1559 (1990).
66. F. Onofri, G. Gréhan, and G. Gouesbet, "Electromagnetic scattering from a multilayered sphere located in an arbitrary beam," Appl. Opt. **34**(30), 7113–7124 (1995).
67. Z. S. Wu, L. X. Guo, K. F. Ren, G. Gouesbet, and G. Gréhan, "Improved algorithm for electromagnetic scattering of plane waves and shaped beams by multilayered spheres," Appl. Opt. **36**(21), 5188–5198 (1997).
68. R. Li, X. Han, L. Shi, K. F. Ren, and H. Jiang, "Debye series for Gaussian beam scattering by a multilayered sphere," Appl. Opt. **46**(21), 4804–4812 (2007).
69. J. J. Wang, G. Gouesbet, G. Gréhan, Y. P. Han, and S. Saengkaew, "Morphology-dependent resonances in an eccentrically layered sphere illuminated by a tightly focused off-axis Gaussian beam: parallel and perpendicular beam incidence," J. Opt. Soc. Am. A **28**(9), 1849–1859 (2011).
70. I. L. Rasskazov, A. Moroz, and P. S. Carney, "Electromagnetic energy in multilayered spherical particles," J. Opt. Soc. Am. A **36**(9), 1591–1601 (2019).
71. S. Schelm and G. B. Smith, "Internal electric field densities of metal nanoshells," J. Phys. Chem. B **109**(5), 1689–1694 (2005).
72. O. B. Toon and T. P. Ackerman, "Algorithms for the calculation of scattering by stratified spheres," Appl. Opt. **20**(20), 3657–3660 (1981).
73. Z. S. Wu and Y. P. Wang, "Electromagnetic scattering for multilayered sphere: recursive algorithms," Radio Sci. **26**(6), 1393–1401 (1991).
74. W. Yang, "Improved recursive algorithm for light scattering by a multilayered sphere," Appl. Opt. **42**(9), 1710–1720 (2003).
75. M. Majic and E. C. Le Ru, "Numerically stable formulation of Mie theory for an emitter close to a sphere," Appl. Opt. **59**(5), 1293–1300 (2020).
76. A. Moroz, "http://wave-scattering.com/codes.html,".
77. https://scattport.org/index.php/light-scattering-software/mie-type-codes.
78. https://www.wgtn.ac.nz/scps/research/research-groups/raman-lab/numerical-tools/sers-and-plasmonics-codes.
79. E. C. Le Ru and P. G. Etchegoin, *Principles of Surface-Enhanced Raman Spectroscopy* (Elsevier, 2009).
80. C. F. Bohren and D. R. Huffman, *Absorption and scattering of light by small particles* (Wiley-VCH Verlag GmbH, Weinheim, Germany, 1998).
81. K. Ladutenko, U. Pal, A. Rivera, and O. Peña-Rodríguez, "Mie calculation of electromagnetic near-field for a multilayered sphere," Comput. Phys. Commun. **214**, 225–230 (2017).
82. http://widgets.nanophotonics.es.
83. https://nanocomposix.com/pages/mie-theory-calculator.
84. https://physics.itmo.ru/en/mie.
85. F. Abelès, "Sur la propagation des ondes électromagnétiques dans les milieux sratifiés," Ann. Phys. **12**(3), 504–520 (1948).
86. F. Abelès, "Recherches sur la propagation des ondes électromagnétiques sinusoïdales dans les milieux stratifiés," Ann. Phys. **12**(5), 596–640 (1950).
87. F. Abelès, "Recherches sur la propagation des ondes électromagnétiques sinusoïdales dans les milieux stratifiés," Ann. Phys. **12**(5), 706–782 (1950).
88. M. Born and E. Wolf, *Principles of optics: Electromagnetic theory of propagation, interference and diffraction of light* (Elsevier, 2013), 6th ed.
89. F. J. García de Abajo and A. Howie, "Retarded field calculation of electron energy loss in inhomogeneous dielectrics," Phys. Rev. B **65**(11), 115418 (2002).
90. U. Hohenester and A. Trügler, "MNPBEM - A Matlab toolbox for the simulation of plasmonic nanoparticles," Comput. Phys. Commun. **183**(2), 370–381 (2012).
91. U. Hohenester, "Simulating electron energy loss spectroscopy with the MNPBEM toolbox," Comput. Phys. Commun. **185**(3), 1177–1187 (2014).

OSA CONTINUUM

92. J. Waxenegger, A. Trügler, and U. Hohenester, "Plasmonics simulations with the MNPBEM toolbox: Consideration of substrates and layer structures," Comput. Phys. Commun. **193**, 138–150 (2015).
93. U. Hohenester, "Making simulations with the MNPBEM toolbox big: Hierarchical matrices and iterative solvers," Comput. Phys. Commun. **222**, 209–228 (2018).
94. J. D. Jackson, *Classical electrodynamics* (John Wiley & Sons, Inc., 1999), 3rd ed.
95. M. Kerker, D.-S. Wang, and H. Chew, "Surface enhanced Raman scattering (SERS) by molecules adsorbed at spherical particles," Appl. Opt. **19**(19), 3373–3388 (1980).
96. M. I. Mishchenko, L. D. Travis, and A. A. Lacis, *Scattering, Absorption, and Emission of Light by Small Particles* (Cambridge University Press, Cambridge, UK, 2002).
97. M. Abramowitz and I. A. Stegun, *Handbook of Mathematical Functions* (Dover Publications, 1973).
98. A. Bott and W. Zdunkowski, "Electromagnetic energy within dielectric spheres," J. Opt. Soc. Am. A **4**(8), 1361–1365 (1987).
99. R. Loudon, "The propagation of electromagnetic energy through an absorbing dielectric," J. Phys. A: Gen. Phys. **3**(3), 233–245 (1970).
100. M. G. Blaber, M. D. Arnold, and M. J. Ford, "Search for the ideal plasmonic nanoshell: the effects of surface scattering and alternatives to gold and silver," J. Phys. Chem. C **113**(8), 3041–3045 (2009).
101. M. A. Ordal, R. J. Bell, R. W. Alexander, L. L. Long, and M. R. Querry, "Optical properties of fourteen metals in the infrared and far infrared: Al, Co, Cu, Au, Fe, Pb, Mo, Ni, Pd, Pt, Ag, Ti, V, and W," Appl. Opt. **24**(24), 4493–4499 (1985).
102. T. J. Arruda and A. S. Martinez, "Electromagnetic energy within magnetic spheres," J. Opt. Soc. Am. A **27**(5), 992–1001 (2010).
103. T. J. Arruda, F. A. Pinheiro, and A. S. Martinez, "Electromagnetic energy within coated spheres containing dispersive metamaterials," J. Opt. **14**(6), 065101 (2012).
104. W. J. Wiscombe, "Improved Mie scattering algorithms," Appl. Opt. **19**(9), 1505–1509 (1980).
105. J. R. Allardice and E. C. Le Ru, "Convergence of Mie theory series: criteria for far-field and near-field properties," Appl. Opt. **53**(31), 7224–7229 (2014).
106. A. Moroz, "Non-radiative decay of a dipole emitter close to a metallic nanoparticle: Importance of higher-order multipole contributions," Opt. Commun. **283**(10), 2277–2287 (2010).
107. A. Moroz, "Electron mean free path in a spherical shell geometry," J. Phys. Chem. C **112**(29), 10641–10652 (2008).
108. R. D. Averitt, S. L. Westcott, and N. J. Halas, "Linear optical properties of gold nanoshells," J. Opt. Soc. Am. B **16**(10), 1824–1832 (1999).
109. R. Ruppin, "Nanoshells with a gain layer: the effects of surface scattering," J. Opt. **17**(12), 125004 (2015).
110. V. I. Zakomirnyi, I. L. Rasskazov, L. K. Sørensen, P. S. Carney, Z. Rinkevicius, and H. Ågren, "Plasmonic nano-shells: atomistic discrete interaction versus classic electrodynamics models," Phys. Chem. Chem. Phys. **22**(24), 13467–13473 (2020).
111. L. Meng, R. Yu, M. Qiu, and F. J. García de Abajo, "Plasmonic nano-oven by concatenation of multishell photothermal enhancement," ACS Nano **11**(8), 7915–7924 (2017).
112. A. K. Kodali, M. V. Schulmerich, R. Palekar, X. Llora, and R. Bhargava, "Optimized nanospherical layered alternating metal-dielectric probes for optical sensing," Opt. Express **18**(22), 23302 (2010).
113. A. K. Kodali, X. Llora, and R. Bhargava, "Optimally designed nanolayered metal-dielectric particles as probes for massively multiplexed and ultrasensitive molecular assays," Proc. Natl. Acad. Sci. **107**(31), 13620–13625 (2010).
114. N. G. Khlebtsov and B. N. Khlebtsov, "Optimal design of gold nanomatryoshkas with embedded Raman reporters," J. Quant. Spectrosc. Radiat. Transfer **190**, 89–102 (2017).
115. J. Y. Lee, A. E. Miroshnichenko, and R.-K. Lee, "Simultaneously nearly zero forward and nearly zero backward scattering objects," Opt. Express **26**(23), 30393–30399 (2018).
116. Z. Ruan and S. Fan, "Superscattering of light from subwavelength nanostructures," Phys. Rev. Lett. **105**(1), 013901 (2010).
117. Z. Ruan and S. Fan, "Design of subwavelength superscattering nanospheres," Appl. Phys. Lett. **98**(4), 043101 (2011).
118. R. Fleury, J. Soric, and A. Alù, "Physical bounds on absorption and scattering for cloaked sensors," Phys. Rev. B **89**(4), 045122 (2014).
119. K. Ladutenko, P. Belov, O. Peña-Rodríguez, A. Mirzaei, A. E. Miroshnichenko, and I. V. Shadrivov, "Superabsorption of light by nanoparticles," Nanoscale **7**(45), 18897–18901 (2015).
120. F. Monticone and A. Alù, "Embedded photonic eigenvalues in 3D nanostructures," Phys. Rev. Lett. **112**(21), 213903 (2014).
121. J. A. Gordon and R. W. Ziolkowski, "The design and simulated performance of a coated nano-particle laser," Opt. Express **15**(5), 2622–2653 (2007).
122. A. E. Miroshnichenko, "Off-resonance field enhancement by spherical nanoshells," Phys. Rev. A **81**(5), 053818 (2010).
123. A. R. Melnyk and M. J. Harrison, "Theory of optical excitation of plasmons in metals," Phys. Rev. B **2**(4), 835–850 (1970).
124. R. Ruppin, "Optical properties of small metal spheres," Phys. Rev. B **11**(8), 2871–2876 (1975).
125. P. T. Leung, "Decay of molecules at spherical surfaces: Nonlocal effects," Phys. Rev. B **42**(12), 7622–7625 (1990).

OSA CONTINUUM

126. Y. Huang and L. Gao, "Superscattering of light from core-shell nonlocal plasmonic nanoparticles," J. Phys. Chem. C **118**(51), 30170–30178 (2014).
127. Y. Eremin, A. Doicu, and T. Wriedt, "Extension of the discrete sources method to investigate the non-local effect influence on non-spherical core-shell particles," J. Quant. Spectrosc. Radiat. Transfer **235**, 300–308 (2019).
128. C. F. Bohren, "Light scattering by an optically active sphere," Chem. Phys. Lett. **29**(3), 458–462 (1974).
129. C. F. Bohren, "Scattering of electromagnetic waves by an optically active spherical shell," J. Chem. Phys. **62**(4), 1566–1571 (1975).
130. D. V. Guzatov and V. V. Klimov, "The influence of chiral spherical particles on the radiation of optically active molecules," New J. Phys. **14**(12), 123009 (2012).
131. M. J. A. de Dood, L. H. Slooff, A. Polman, A. Moroz, and A. van Blaaderen, "Modified spontaneous emission in erbium-doped SiO2 spherical colloids," Appl. Phys. Lett. **79**(22), 3585–3587 (2001).
132. M. J. A. de Dood, L. H. Slooff, A. Polman, A. Moroz, and A. van Blaaderen, "Local optical density of states in SiO2 spherical microcavities: Theory and experiment," Phys. Rev. A **64**(3), 033807 (2001).
133. P. R. Wiecha, A. Arbouet, A. Cuche, V. Paillard, and C. Girard, "Decay rate of magnetic dipoles near nonmagnetic nanostructures," Phys. Rev. B **97**(8), 085411 (2018).
134. I. L. Rasskazov, P. S. Carney, and A. Moroz, "Stratify: a comprehensive and versatile matlab code for a multilayered sphere," (2020) [retrieved 11 August 2020]. https://gitlab.com/iliarasskazov/stratify